Removal of Rhodamine B from aqueous solution using magnetic NiFe nanoparticles

Yan Liu, Kaige Liu, Lin Zhang and Zhaowen Zhang

ABSTRACT

Surface-modified magnetic nano alloy particles $Ni_{2.33}Fe$ were prepared using a hydrothermal method and they were utilized for removing Rhodamine B (RhB) from aqueous solution. The magnetic nanoparticles were characterized by X-ray diffraction, scanning electron microscopy, thermogravimetric analysis and Fourier transform infrared spectroscopy, which confirmed that the surface of the magnetic product with a face-centered cubic-type structure was successfully modified by sodium citrate. Kinetics studies were conducted. The pseudo-second-order kinetic model was used for fitting the kinetic data successfully. The Freundlich and Langmuir adsorption models were employed for the mathematical description of adsorption equilibrium. It was found that the adsorption isotherm can be very satisfactorily fitted by the Freundlich model.

Key words | adsorption, Freundlich adsorption model, kinetics, magnetic alloy particles, Rhodamine B

Yan Liu (corresponding author)
Kaige Liu
Lin Zhang
Zhaowen Zhang
College of Materials and Metallurgy,
Northeastern University,
Shenyang 110004,
China
E-mail: *liuy@smm.neu.edu.cn*

INTRODUCTION

It is known that industrial wastewater containing organic compounds, especially phenyl, lead to a risk to humans, even at a low concentration (Petrova *et al.* 2010; Jin *et al.* 2011). Most of the organic contaminant is stable and hard to degrade in natural conditions. Thus, how to effectively and deeply remove these hazardous pollutants from the water system is a crucial but challenging task. Nowadays, some approaches have been developed and utilized to remove organic pollutants from wastewaters, such as coagulation/flocculation (Ahammed *et al.* 2014), chemical precipitation (Zhu *et al.* 2007), membrane filtration (Zheng *et al.* 2013), catalytic and photocatalytic oxidation (Copper & Burch 1999; Larachi *et al.* 2001), chlorination (Sinkkonen *et al.* 1997), reverse osmosis (Arzuada *et al.* 2008) and adsorption (Anbia & Lashgari 2010).

Rhodamine B (RhB) is widely used in textiles and foodstuffs as one of the most important colorants. It is toxic and carcinogenic, and its biological degradation is slow. It has been reported that some methods were capable of removing RhB from wastewater. Bao *et al.* (2014) prepared a selective photocatalyst (RhB-MIP/TiO_2) and it displayed strong affinity and high adsorption capacity for RhB. Lei *et al.* (2012) demonstrated that a catalyst (graphene–TiO_2) exhibited superior adsorptivity and sonocatalytic activity under ultrasonic irradiation for the decomposition of RhB. Machado *et al.* (2012) used ozonization to treat dye wastewaters containing RhB. However, the processes have not been used extensively because of high cost, complex technology and relatively harsh reaction conditions.

Adsorption is recognized as an effective and economic method for wastewater treatment. But for traditional adsorbents, such as activated carbon, chitosan, zeolites and clays, the relatively low adsorbing efficiency limits their further utilization. Nano-materials exhibit better adsorption capacity because of their large surface areas and high activities caused by the size quantization effect. However, the problem is that although the smaller size of the particles made them favorable to adsorb, they are more difficult to isolate from the water. The nanoparticles dissolved in the water can cause more problems (Bystrzejewska-Piotrowskaa *et al.* 2009). Magnetic separation has been shown to be a very promising method for solid–liquid phase. Such easy separation is essential to improve the operation efficiency and reduce the cost during wastewater treatment. Hence, magnetic nanoparticles attract increasing attention in comparison with other nano-materials. For example, ferriferous oxide (Yuan *et al.* 2010) has been reported as a magnetic adsorbent for removal of pollutants. But these nano-magnetic oxides easily lose magnetism as a result of being oxidized. Our study showed that nano NiFe magnetic

doi: 10.2166/wst.2015.319

alloy materials are far superior to iron oxides in oxidation resistance (Liu *et al.* 2014). Therefore, they have more potential to be used repeatedly as magnetic adsorbents.

In this study, a novel surface-modified NiFe magnetic adsorbent was synthesized and used for the removal of RhB from wastewater. The advantages of low toxicity, eco-friendliness and easily recycling were presented by the NiFe magnetic particles.

METHODS

Preparation of NiFe nanoparticles

Ferrous sulfate ($FeSO_4$•$7H_2O$, 99.5%), nickel(II) chloride ($NiCl_2$•$6H_2O$), sodium citrate (Cit, 99%), sodium hydroxide (NaOH), hydrazine hydrate (H_2NNH_2•H_2O) and glycol ethylene ($HOCH_2CH_2OH$) were analytical-reagent grade. All chemicals were used as received. Deionized water was used in all experiments.

Typically, 1.4850 g of $FeSO_4$•$7H_2O$, 3.8100 g of $NiCl_2$•$6H_2O$ and 62.8490 g of sodium citrate were dissolved in 296.5 mL of deionized water. Thirty-two millilitres of 1 mol/L NaOH was added to the solution to adjust pH to around 12.5; 2.8 mL of glycol ethylene was used as surfactant and 18.7 mL of hydrazine hydrate was dropped into the solution as reducing agent. The mixture solution was transferred to an autoclave after being stirred well under N_2. The autoclave was sealed and put into a furnace which was preheated to 120 °C. The autoclave was cooled to room temperature after heating for 19 h. NiFe nanoparticles were separated from the solution with a magnetic bar. The products obtained were cleaned and re-dispersed in deionized water and ethanol several times.

Characterization

X-ray diffraction (XRD) patterns were recorded by a Rigaku D/MAX 2500 diffractometer, equipped with a graphite-monochromatized Cu Kα radiation course ($\lambda = 0.154$ nm). Scanning electron microscopy (SEM) was performed using a Zeiss Ultra Plus model operating at an acceleration voltage of 15 kV. A Lakeshore Model 7407 vibrating sample magnetometer (VSM) was used for magnetization measurement at room temperature. Thermogravimetric (TG) analysis was performed on a TA Instruments SDT Q600. The rate of temperature change was 10 °C/min. Fourier transform infrared spectroscopy (FT-IR) measurements were performed on a Perkin–Elmer Spectrum 100 to identify the vibration frequency in the functional groups of the materials.

Adsorption experiments

For the equilibrium experiment, 100 mg of $Ni_{2.33}Fe$ nanoparticles was added into 30 mL of RhB solution at a series of known initial concentrations (C_0). After stirring the samples for 24 h with an agitator, the magnetic particles were separated using a magnet from the solution. The equilibrium concentration of RhB in the solution (C_e) was determined by UV–visible spectrophotometry at 556 nm.

The amount of the adsorbed pollutants on the magnetic adsorbents was calculated with Equation (1)

$$q_e = \frac{(C_0 - C_e)}{m} \times V \quad (1)$$

where q_e is adsorbed amount on the adsorbents (mg/g), C_0 and C_e are expressed in mg/mL, V is the solution volume (mL) and m is the adsorbents mass (g).

For kinetic experiments, 200 mg of $Ni_{2.33}Fe$ nanoparticles was added into 200 mL of RhB solution with different initial concentrations (20 mg/L, 45 mg/L, 90 mg/L, 135 mg/L and 200 mg/L, respectively). The solution was stirred and sampled at appropriate time intervals.

RESULTS AND DISCUSSION

Characterization of magnetic nanoparticles

The compositions of Ni and Fe in the as-synthesized products were determined using the inductively coupled plasma optical emission spectrometry (ICP-OES) method. The ratio of Ni to Fe was 2.33:1, and so the magnetic product was expressed as $Ni_{2.33}Fe$.

The as-synthesized bimetallic particles were characterized by XRD, and the XRD pattern is shown in Figure 1.

The peaks, at 44.36°, 51.72° and 76.15°, can be indexed to (111), (200) and (220) planes characteristic of a NiFe alloy with a face-centered cubic (fcc) type of structure (Liu *et al.* 2014). The size value calculated based on the peak width using the Scherrer equation is 11.90 nm.

According to the results of ICP and XRD, it can be deduced that the structure of the products is an fcc-type NiFe alloy based on fcc-type Ni where part of the Ni was substituted by Fe atoms.

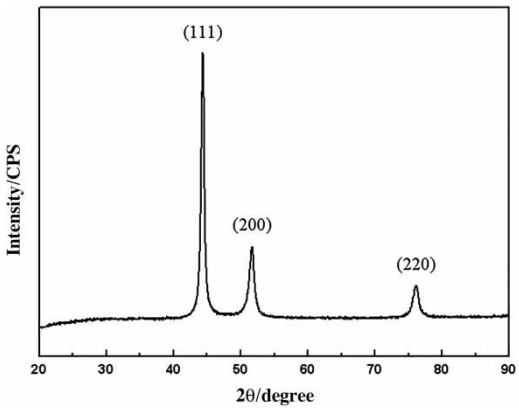

Figure 1 | XRD pattern of $Ni_{2.33}Fe$.

Figure 2 shows a representative set of SEM images for the as-synthesized $Ni_{2.33}Fe$ particles. The shapes of particles have chainlike (Figure 2(a)) and spherical (Figure 2(b)) structures. More details can be observed in the magnified images from their higher magnification micrographs (Figure 2). The diameter of chainlike wires is about 1 μm, the length ranges from dozens to hundreds of microns, and the wires are interconnected. The surface of the chainlike product (insert (a)) is aristate. In insert (b), the particles appear near-spherical, smooth, uneven and agglomerated.

The TG for the particles of $Ni_{2.33}Fe$ is shown in Figure 3. A weight loss of about 4.7% was observed below 400 °C which is attributed to the loss of adsorbed water or ethylene molecules on the surface of particles. A sharp weight increase took place at the temperature of approximately 400 °C and all the way up to 718 °C due to the oxidation of metal Fe and Ni in the alloy. Again a weight loss appeared at 718 °C. It can be deduced that the loss resulted from the decomposition of sodium citrate coordinated on the surface of the particles. The weight loss can be also an indication that sodium citrate has affinity to the surface of the $Ni_{2.33}Fe$ alloy to change the surface property of the alloy particles due to the amount of sodium citrate used in the reaction.

The detection of IR spectra of $Ni_{2.33}Fe$ and sodium citrate proved the existence of sodium citrate in the as-synthesized $Ni_{2.33}Fe$ particles. By comparing the IR curves (in Figure 4), it can be obviously seen that there is a strong stretching vibration peak of C═O at 1,623 nm and C—O at 1,106 nm in curve 'b' and the two characteristic peaks of sodium citrate appeared at the same peaks as in curve 'a'. This is further evidence that sodium citrate has affinity to the surface of $Ni_{2.33}Fe$.

The magnetic properties were characterized using VSM at room temperature. The values of the remanence,

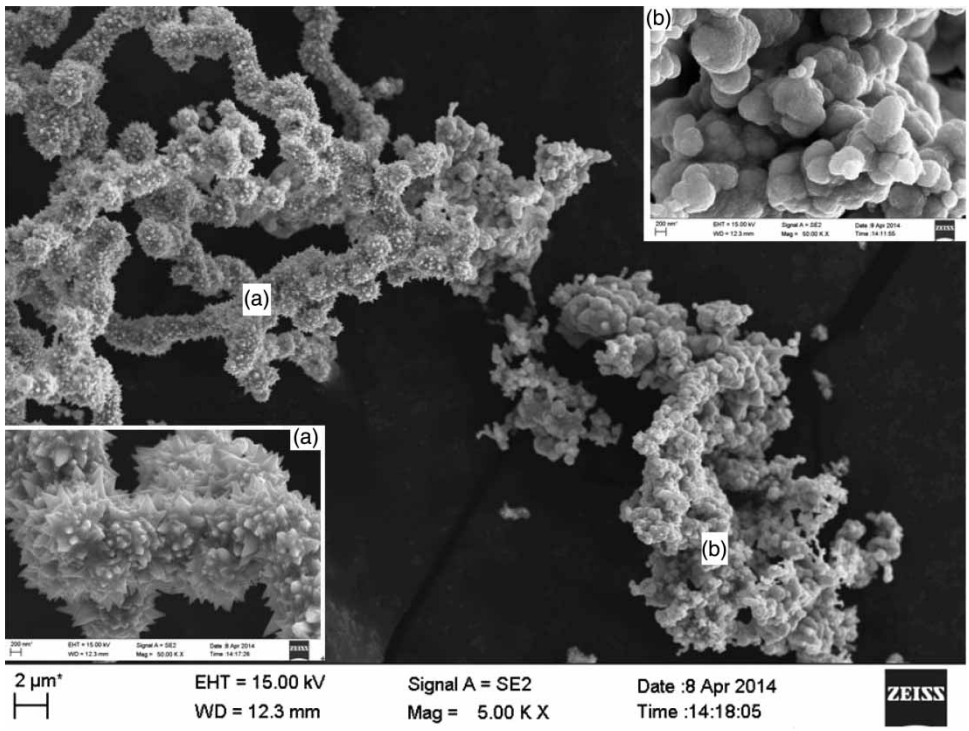

Figure 2 | SEM images of $Ni_{2.33}Fe$ (insert graph: magnified images for part (a) and part (b)).

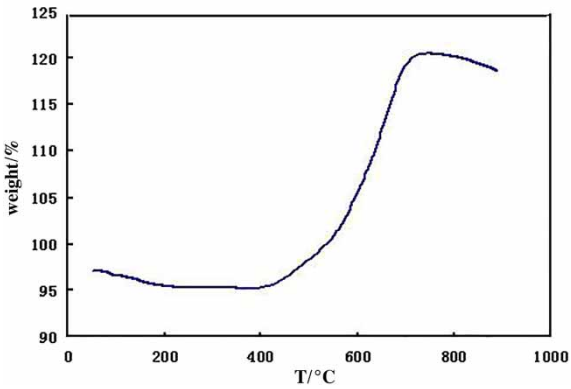

Figure 3 | Thermogravimetric curves for nanoparticles.

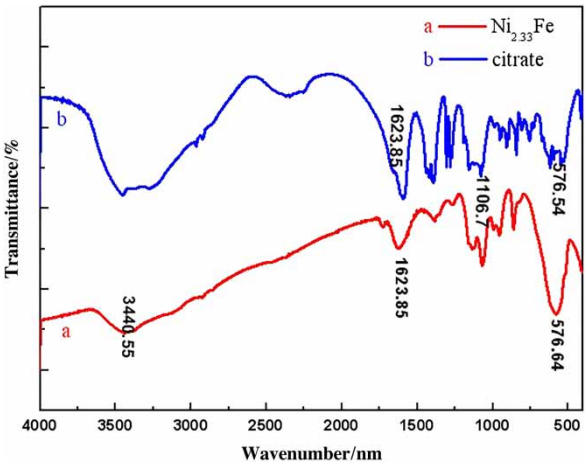

Figure 4 | IR spectra of nanoparticles $Ni_{2.33}Fe$ and sodium citrate.

saturation magnetization and coercivity are 2.91 emu/g, 75.44 emu/g and 45.9 Oe, respectively.

Adsorption of RhB

Adsorption kinetics

Adsorption dynamics of RhB onto nanomagnetic particles of $Ni_{2.33}Fe$ was investigated at different initial solute concentrations and the results are shown in Figure 5. Fast adsorptions took place in 30 min and adsorption equilibriums were completed within the contact time of 24 h. For example, at initial solute concentration of 45 mg/L, the concentration decreased by 1.13 mg/L within 30 min, which was about 70% of total amounts adsorbed when adsorption reached equilibrium. The equilibrium adsorption quantity increased with the increase of the initial concentration.

A contrast adsorption experiment was done using the particle of $Ni_{3.54}Fe$ (Liu *et al.* 2014). $Ni_{3.54}Fe$ was synthesized

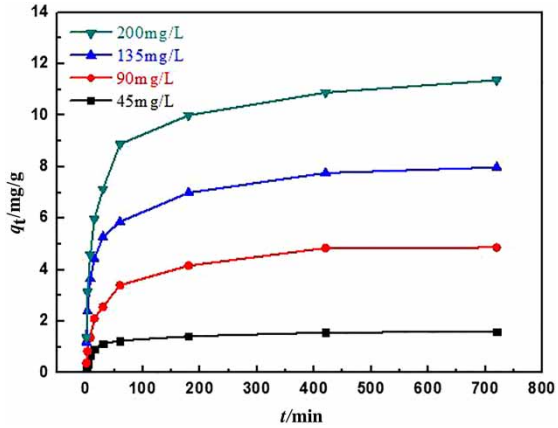

Figure 5 | Effect of contact time on the adsorption of RhB onto nanomagnetic $Ni_{2.33}Fe$ particles at different RhB initial concentrations.

using the same method as for $Ni_{2.33}Fe$ in this study, except the usage of sodium citrate. For $Ni_{3.54}Fe$ particle, the molar ratio of sodium citrate to metal (Ni + Fe) was 0.2:1, but for $Ni_{2.33}Fe$, the ratio was 10:1. $Ni_{3.54}Fe$ exhibited zero adsorption ability. It was because sodium citrate did not grow on the surface of the particles due to the low usage.

The pseudo-first-order kinetic equation and pseudo-second-kinetic equation often are used to model the experiment data (Arasteh *et al.* 2010; Irama *et al.* 2010). The pseudo-first-order kinetic is written as

$$\log(q_e - q_t) = \log(q_e) - \frac{Kt}{2.303} \tag{2}$$

The pseudo-second-order equation is expressed as follows:

$$\frac{t}{q_t} = \frac{1}{k'q_e^2} + \frac{1}{q_e}t \tag{3}$$

where q_e and q_t (mg/g) are the amount of $Ni_{2.33}Fe$ adsorbed at equilibrium and at time t, respectively. K is the kinetic constant of pseudo-first-order adsorption (min^{-1}) and k' is the pseudo-second-order rate constant (g/(mg min)).

If the second-order kinetic equation is applicable, the plot of t/q_e against t of Equation (3) should give a linear relationship. The q_e and k' can be determined by the slope and intercept of the plot.

The data of Figure 5 were potted according to the pseudo-second-order model (Equation (3)) (shown in Figure 6); the corresponding adsorption parameters of the pseudo-first-order model and pseudo-second-order model are presented in Table 1.

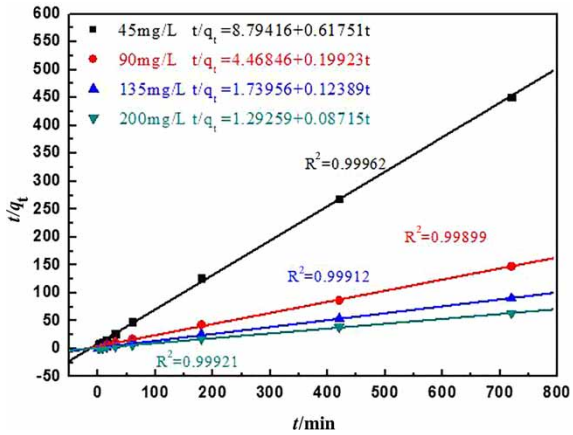

Figure 6 | Plot of pseudo-second-order model at different concentrations of RhB for $Ni_{2.33}Fe$ as adsorbent.

The regression coefficient values (R^2) in the pseudo-second-order model ($R^2 > 0.999$) are larger than in the pseudo-first-order model, which indicates that the pseudo-second-order model is more suitable to describe the adsorption. Moreover, the theoretical q_e values calculated from the pseudo-first-order model have higher deviations than the experimental q_e values at different initial adsorbate concentrations. However, the theoretical q_e values predicted by the pseudo-second-order model are the nearest to the experimental q_e values. The results suggest that RhB adsorbed by $Ni_{2.33}Fe$ magnetic nanoparticles do not follow the pseudo-first-order model but fit the second-order equation for the adsorption of RhB onto nano-$Ni_{2.33}Fe$.

Adsorption mechanism

The intraparticle diffusion model based on the theory proposed by Weber and Morris was tested as (Arasteh *et al.* 2010)

$$q_t = K_d t^{1/2} + C \tag{4}$$

where K_d (mg/(g min$^{1/2}$)) is the intraparticle diffusion rate constant and C (mg/g) is a constant related to the thickness of the boundary layer.

The diffusion model plots are shown in Figure 7. If the so-called Weber-Morris plot of q_t versus $t^{1/2}$ gives a straight line, the adsorption process is controlled by intraparticle diffusion only. However, if the data exhibit multi-linear plots, two or more steps influence the sorption process. The first steeper portion is the external surface adsorption or instantaneous adsorption stage. The second portion is the gradual adsorption stage, where the intraparticle diffusion is rate limited (Arasteh *et al.* 2010). From the slopes of the two processes, intraparticle diffusion is rate limited but all straight lines do not pass the original point. Thus it suggests that in the adsorption of RhB over the nano-$Ni_{2.33}Fe$ is controlled by external mass transfer followed by intraparticle diffusion mass transfer.

It also can be deduced from values of K_{di} and C_i shown in Table 2 that the adsorption process is controlled by intraparticle diffusion because K_{d1} is larger than K_{d2}, while C_1 is smaller than C_2 (Guo *et al.* 2014).

Adsorption isotherms

The equilibrium data were fitted to Langmuir and Freundlich isotherm equations (Banerjee & Chen 2007).

The Langmuir equation can be expressed as

$$\frac{C_e}{q_e} = \frac{C_e}{q_m} + \frac{1}{q_m K_L} \tag{5}$$

The linear form of the Freundlich equation, which is an empirical equation used to describe heterogeneous adsorption systems, can be represented as follows:

$$\ln q_e = \ln K_F + \frac{1}{n} \ln C_e \tag{6}$$

Table 1 | Kinetic model constants determined by the adsorption of RhB onto $N_{2.33}Fe$ at different initial concentrations

		Pseudo-first-order			Pseudo-second-order		
C_0 (mg/L)	q_e (mg/g) experimental	K (min^{-1})	R^2	q_e (mg/g) calculated	K' (g/(mg min))	R^2	q_e (mg/g) calculated
45	1.596	0.00543	0.9139	0.8117	0.04336	0.9996	1.6194
90	4.869	0.00498	0.8922	3.0665	0.00888	0.9989	5.0193
135	7.98	0.00566	0.9560	4.2007	0.00882	0.9991	8.0717
200	11.3655	0.00576	0.9514	6.2003	0.00588	0.9992	11.4745

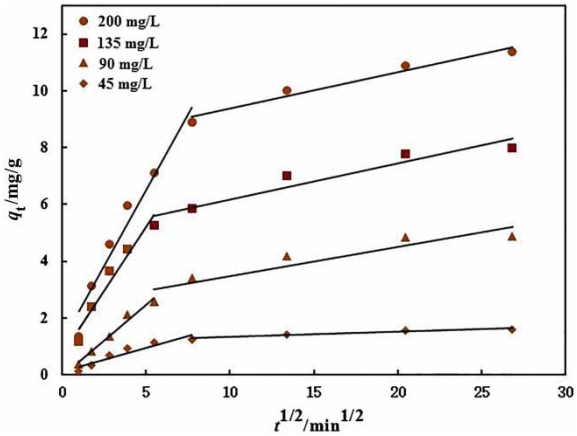

Figure 7 | Weber-Morris intraparticle diffusion plots for RhB onto $Ni_{2.33}Fe$ at different concentrations of RhB.

Table 2 | The intraparticle diffusion parameters for Rhb adsorption onto $Ni_{2.33}Fe$

Initial concentration (mg/L)	K_{d1} (mg/(g min$^{1/2}$))	C_1 (mg/g)	R^2	K_{d2} (mg/(g min$^{1/2}$))	C_2 (mg/g)	R^2
45	0.167	0.109	0.900	0.0184	1.141	0.925
90	0.501	0.046	0.978	0.079	2.970	0.887
135	0.894	0.720	0.949	0.110	5.270	0.912
200	1.062	1.165	0.544	0.129	8.071	0.963

where q_m is the maximum capacity of adsorbent (mg/g), K_L is the Langmuir adsorption constant, K_F is the Freundlich constant, and n is the heterogeneity factor.

The equilibrium adsorption capacities of RhB are expressed by Langmuir and Freundlich isotherm equations (Equations (5) and (6)), and the results of the data fitting are shown in Figure 8. In the Langmuir model (Figure 8(a)), given that the regression coefficient $R^2 = 0.7069$, is low, and the slope of the line is a negative value, the value of q_m would become unreasonably negative. This implies that the Langmuir model cannot represent the data reasonably well. As the Langmuir describes monolayer adsorption, this also indicates the monolayer adsorption is not suitable for the adsorbing of RhB over $Ni_{2.33}Fe$.

The regression coefficient of R^2 is 0.991 based on the data fitted for the Freundlich model (Figure 8(b)). It is apparent that the Freundlich equation agrees very well while the Langmuir equation gives a poorer fit. Thus, the adsorption of RhB on the $Ni_{2.33}Fe$ obeys the Freundlich adsorption isotherm. The values of K_F and $1/n$, 0.0113 and 1.359, respectively, were determined from the slope and intercept of the linear plot of $\ln q_e$ versus $\ln C_e$. The value of $1/n$ greater than 1 indicated that RhB can be adsorbed by the magnetic $Ni_{2.33}Fe$.

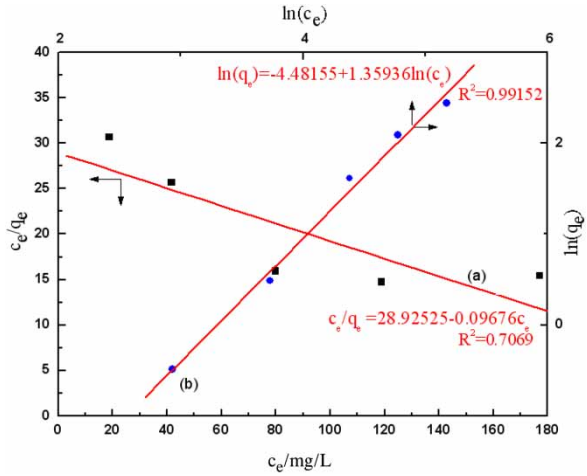

Figure 8 | Adsorption isotherms of RhB onto nano-$Ni_{2.33}Fe$. Fitting models: (a) Langmuir; (b) Freundlich.

CONCLUSION

Magnetic $Ni_{2.33}Fe$ alloy particles with fcc-type structure were prepared. The surface of the alloy particles has affinity to sodium citrate. The adsorbing action of RhB onto nano-$Ni_{2.33}Fe$ was investigated. Adsorption kinetics was found to be well predicted by the pseudo-second-order kinetic model. The adsorption process is controlled by external mass transfer followed by intraparticle diffusion mass transfer. The adsorption process can be described by the Freundlich isotherm.

ACKNOWLEDGEMENTS

The research work was supported by the University Student Innovation Research and Training Program of China (140088), the Natural Science Foundation of Liaoning Province of China (2013020104) and the National Natural Scientific Foundation of China (Grant No. 51574084).

REFERENCES

Ahammed, S., Ajoy, S., Gajbhiye, V., Suman, G., Manjaiah, K. & Eldho, V. 2014 Simultaneous removal of multiple pesticides from water: effect of organically modified clays as coagulant aid and adsorbent in coagulation–flocculation process. *Environmental Technology* **35** (20), 2619–2627.

Anbia, M. & Lashgari, M. 2010 Synthesis of amino-modified ordered mesoporous silica as a new nano sorbent for the removal of chlorophenols from aqueous media. *Chemical Engineering Journal* **150** (2–3), 555–560.

Arasteh, R., Masoumi, M., Rashidi, A., Moradi, L., Samimi, V. & Mostafavi, S. 2010 Adsorption of 2-nitrophenol by multi-wall carbon nanotubes from aqueous solutions. *Applied Surface Science* **256** (14), 4447–4455.

Arzuada, J., Lopez-Munoz, M. & Aguado, J. 2008 Temperature, pH and concentration effects on retention and transport of organic pollutants across thin-film composite nanofiltration membranes. *Desalination* **221** (1–3), 253–258.

Banerjee, S. & Chen, D. 2007 Fast removal of copper ions by gum Arabic modified magnetic nano-adsorbent. *Journal of Hazardous Materials* **147** (3), 792–799.

Bao, L., Meng, M., Sun, K., Li, W., Zhao, D., Li, H. & He, M. 2014 Selective adsorption and degradation of Rhodamine B with modified titanium dioxide photocatalyst. *Journal of Applied Polymer Science* **131** (20), DOI: 10.1002/app.40890.

Bystrzejewska-Piotrowska, G., Golimowski, J. & Urban, P. 2009 Nanoparticles: their potential toxicity, waste and environmental management. *Waste Management* **29** (9), 2587–2595.

Copper, C. & Burch, R. 1999 An investigation of catalytic ozonation for the oxidation of halocarbons in drinking water preparation. *Water Research* **33** (18), 3695–3700.

Guo, J., Li, B., Liu, L. & Lv, K. 2014 Removal of methylene blue from aqueous solutions by chemically modified bamboo. *Chemosphere* **111**, 225–231.

Iram, M., Guo, C., Guan, Y., Ishfaq, A. & Liu, H. 2010 Adsorption and magnetic removal of neutral red dye from aqueous solution using Fe_3O_4 hollow nanospheres. *Journal of Hazardous Materials* **181** (1–3), 1039–1050.

Jin, X., Yu, C., Li, Y., Qi, Y., Yang, L., Zhao, G. & Hu, H. 2011 Preparation of novel nano-adsorbent based on organic–inorganic hybrid and their adsorption for heavy metals and organic pollutants presented in water environment. *Journal of Hazardous Materials* **186** (2–3), 1672–1680.

Larachi, F., Ihuta, I. & Belkacemi, K. 2001 Catalytic wet air oxidation with a deactivating catalyst analysis of fixed and sparked three-phase reactors. *Catalysis Today* **64** (3–4), 309–320.

Lei, Z., Trisha, G., Park, C., Meng, Z. & Won-Chun, O. 2012 Enhanced sonocatalytic degradation of Rhodamine B by graphene-TiO_2 composites synthesized by an ultrasonic-assisted method. *Chinese Journal of Catalysis* **33** (18), 1276–1283.

Liu, Y., Chi, Y., Shan, S., Yin, J., Luo, J. & Zhong, C. 2014 Characterization of magnetic NiFe nanoparticles with controlled bimetallic composition. *Journal of Alloys and Compounds* **587**, 260–266.

Machado, E., Dambros, V., Kist, L., Lobo, E., Tedesco, S. & Moro, C. 2012 Use of ozonization for the treatment of dye wastewaters containing Rhodamine B in the agate industry. *Water Air Soil Pollution* **223** (4), 1753–1764.

Petrova, B., Budinova, T., Tsyntsarski, B., Kochkodan, V., Shkavro, Z. & Petrov, N. 2010 Removal of aromatic hydrocarbons from water by activated carbon from apricot stones. *Chemical Engineering Journal* **165** (1), 258–264.

Sinkkonen, S., Rantion, T., Paasivitra, J., Peltonen, S., Vattulainen, A. & Lammi, R. 1997 Chlorinated phenolic compound in coniferous needles. Effects of metal and paper industry and incineration. *Chemosphere* **35** (6), 1175–1185.

Yuan, P., Liu, D., Fan, M., Yang, D., Zhu, R., Ge, F., Zhu, J. & He, H. 2010 Removal of hexavalent chromium [Cr(VI)] from aqueous solutions by the diatomite-supported/unsupported magnetite nanoparticles. *Journal of Hazardous Materials* **173** (1–3), 614–621.

Zheng, Y., Yao, G., Cheng, Q., Yu, S., Liu, M. & Gao, C. 2013 Positively charged thin-film composite hollow fiber nanofiltration membrane for the removal of cationic dyes through submerged filtration. *Desalination* **328**, 42–50.

Zhu, M., Lee, L., Wang, H. & Wang, Z. 2007 Removal of an anionic dye by adsorption/precipitation processes using alkaline white mud. *Journal of Hazardous Materials* **149** (3), 735–741.

First received 18 March 2015; accepted in revised form 3 June 2015. Available online 30 June 2015